Unsteady Low-Speed Aerodynamic Model for Complete Aircraft Configurations

Joseph Katz*
NASA Ames Research Center, Moffett Field, California
and
Brian Maskew†
Analytical Methods Inc., Redmond, Washington

A method for converting steady-state, potential-flow based panel methods into a time-dependent mode is derived and applied to several test cases. For this development, an improved vortex wake model was constructed that was also suitable for simulating the leading edge separation of slender wings at high angles of attack. Computed flow-field simulations are presented for various unsteady and high-angle-of-attack conditions, involving geometries such as simple wings, rotors, and complete aircraft configurations.

Nomenclature

A_{ij}, B_{ij}, C_{ij} = influence coefficients
AR = aspect ratio (wing area/b^2)
b = wingspan
c = wing reference chord
C_L = lift coefficient (lift/$0.5\rho V_\infty^2 S$)
$C_{\ell R}$ = rotor section lift coefficient [section lift/$0.5\rho(R\dot{\psi})^2 c$]
C_m = pitching moment coefficient (pitching moment/$0.5\rho V_\infty^2 Sc$)
$C_{m\dot{\alpha}}$ = pitch damping coefficient
C_p = pressure coefficient ($p - p_\infty/0.5\rho V_\infty^2$)
C_r = rolling moment coefficient [rolling moment/$0.5\rho V_\infty^2 S(b/2)$]
G_1, G_2 = relative translation and rotation of the origin
h = amplitude of heaving oscillations
M_{TIP} = rotor tip Mach number
n = vector normal to panel surface
p = pressure
R = rotor radius
r = vector (x, y, z)
S = reference area
s = area element
t = time
U, V, W, = velocity components, measured in inertial frame
V_f = momentary local velocity in the X, Y, Z frame
v = velocity, defined in Eq. 9
v_f = momentary local velocity in the x, y, z frame
v_N = transpiration velocity, normal to panel surface
v_{rel} = relative velocity, measured in the x, y, z frame
V_∞ = freestream velocity
X, Y, Z = inertial coordinates
x, y, z = body coordinates
α = angle of attack
α_R = rotor blade angle of attack
α_1 = amplitude of pitch oscillations
Γ = circulation
θ = rotation about the y axis
μ = doublet strength
ρ = air density
σ = source strength
Φ = velocity potential
ϕ = rotation about the x axis
ψ = rotation about the z axis
Ω = rotation rate of body-coordinates
ω = oscillation frequency

Subscripts

o = origin
w = wake
∞ = freestream condition

Introduction

IN the course of developing computational methods to analyze complex aircraft maneuvers, the simulation of unsteady aerodynamics and the resulting wake dynamics is still an intriguing challenge. This time-dependent fluid-dynamic modeling capability is much needed in aeronautical disciplines such as flight dynamics and flight simulation, and for time-dependent structural load analysis. Computation of a vehicle's stability derivatives, for example, at the first stages of shape development will then allow early flight simulation and evaluation of flying qualities. This capability will also result in benefits at the more advanced phases of prototype testing where experimental derivation of these stability derivatives is still limited and costly. Models of vortex wake motion can contribute too, to the investigation of leading-edge (LE) flow-separation from swept-wings, as would occur during high-angle-of-attack landings or maneuvering of high-speed vehicles. Similarly, estimation of rotorcraft vortex wake position can shed light on some of the more complex problems associated with a helicopter's flight.

Detailed solution of the complete nonlinear fluid dynamic equations along time-dependent flight paths is still in its initial phases.[1] The expansion of the computational grid to encompass large wake histories along curved, arbitrary path coordinates will only complicate the computation and make it more costly. An alternative approach, which will be followed here, postulates the use of simplified fluid dynamic equations while retaining the three-dimensional nature of both an aircraft geometry and its flight path. Such simplified fluid dynamic solutions were developed during the past years for inviscid steady flows,[2-10] and were successful in simulating high

Presented as Paper 86-2180 at the AIAA Atmospheric Flight Mechanics Conference, Williamsburg, VA, Aug. 18-20, 1986; received Sept. 27, 1986; revision received July 6, 1987.

*NRC Senior Research Associate; currently Professor, Department of Aerospace Engineering, San Diego State University, San Diego, CA. Member AIAA.
†Vice President. Member AIAA.

Reynolds number, lifting, nonseparated, subsonic or supersonic[2,5,8] flows. An additional advantage of this potential formulation lies in the use of Green's integral theorem.[3] This results in an integral equation which is then solved on the body's boundaries only, rather than over a complex grid spanning the whole fluid volume. Detailed description of the mathematical principles and of the numerical schemes used in these models are provided in Refs. 5–7 and Ref. 10. These methods were extended to include periodic wing oscillations,[7] higher-order singularity elements,[8,10] iteration with viscous boundary layer solutions,[9] wake rollup relaxations and jet models,[11] to cope with a variety of V/STOL aircraft and helicopter-related[4] problems.

In this present study, a potential (panel) method is used together with a time-dependent vortex wake model to simulate the shear layers emanating from the separation lines. These separation lines lie along wing trailing edges or along lines whose location is known from experiments, as in the case of flow separation from wings with highly swept-back and sharp LE. The combination of a well-developed panel code[9] with this unsteady vortex wake model resulted in two improvements: 1) the computation of the loads during arbitrary time-dependent aircraft motion were made possible, and 2) since the timewise, step-by-step construction of vortex wakes is numerically stable, the simulation of LE separation from highly swept wings (at high angles of attack) was obtained.

Model

Basic Formulation and Choice of Coordinates

Computation of the aerodynamic response to a set of aircraft control inputs requires the coupled solution of the flowfield and vehicle's inertial equations. At the present state, however, the aircraft motion history is assumed to be known and the motion of the body-fixed coordinate system (x, y, z), as shown in Fig. 1, is prescribed. Let (X, Y, Z) be an inertial frame that coincides with the (x, y, z) frame of reference at $t = 0$. Then, at $t > 0$, the relative motion of the origin $(\ )_o$ of the body fixed frame of reference is prescribed by $G_1(t)$, and the momentary rotation angles (ϕ, θ, ψ) are prescribed by $G_2(t)$.

$$(X_o, Y_o, Z_o) = G_1(t) \tag{1}$$

$$(\phi, \theta, \psi) = G_2(t) \tag{2}$$

The fluid surrounding the aircraft is assumed to be inviscid, irrotational, and incompressible over the entire flowfield, excluding the vehicle's solid boundaries and its wakes. Therefore, a velocity potential Φ can be defined and the continuity equation, in the inertial frame of reference, becomes

$$\nabla^2\Phi = 0 \tag{3}$$

with the first boundary condition requiring zero normal velocity across the body's solid boundaries,

$$\nabla\Phi \cdot n - V_f \cdot n = 0 \tag{4}$$

where V_f is the kinematic velocity, as viewed from the inertial frame. The second boundary condition requires that the flow disturbance, due to the body's motion through the fluid, should diminish far from the aircraft,

$$\lim \nabla\Phi_{r\to\infty} = 0 \tag{5}$$

where $r = (x, y, z)$. Along the wing's trailing edges the velocity has to be limited in order to fix the rear stagnation line and therefore

$$\nabla\Phi < \infty \text{ (at trailing edges)} \tag{6}$$

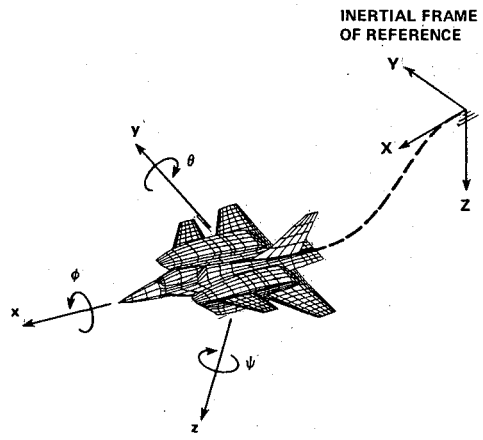

Fig. 1 Definition of coordinate systems.

and in the potential flow region the angular momentum can not change, thus the circulation Γ is conserved.

$$\frac{d\Gamma}{dt} = 0 \text{ (for any } t) \tag{7}$$

The solution of this problem, which becomes time-dependent because of boundary condition (4), is easier in the body-fixed coordinate system (e.g., the velocity normal to the body's solid boundaries becomes zero). Consequently, a transformation f between the two coordinate systems has to be established, based on the flight path information of Eqs. (1) and (2).

$$\begin{pmatrix} x \\ y \\ z \end{pmatrix} = f(X_o, Y_o, Z_o, \phi, \theta, \psi)\begin{pmatrix} X \\ Y \\ Z \end{pmatrix} \tag{8}$$

similarly the transformation of the velocities is

$$v = V_o + v_{\text{rel}} + \Omega \times r \tag{9}$$

where V_o is the velocity of the (x, y, z) systems origin, $\Omega = (\dot\phi, \dot\theta, \dot\psi)$, and $v_{\text{rel}} = (\dot x, \dot y, \dot z)$. The transformation of Eqs. (3), (5), and (6) into the aircraft frame of reference will not change them and the continuity equation remains

$$\nabla^2\Phi = 0 \text{ (in body fixed coordinates)} \tag{10}$$

Boundary condition (4), however has to take into account the transformed velocity v_f of Eq. (9) and thus becomes

$$\nabla\Phi \cdot n = v_f \cdot n \tag{11a}$$

In order to model nonzero velocities across the boundaries, a transpiration velocity v_N is added, so engine inlet/exit flows or boundary layer displacement can be modeled:[9]

$$\nabla\Phi \cdot n = v_f \cdot n + v_N \tag{11b}$$

The most important conclusion from these results is that for incompressible flows the instantaneous solution is independent of time. That is, since the speed of sound is assumed to be infinite, the influence of the momentary boundary condition is immediately radiated across the whole fluid region. Therefore, steady-state solutions (such as panel methods) can be used to treat the time-dependent problem by substituting the instantaneous boundary condition [Eq. (11a)] at each moment. The wake shape, however, does depend on the time history of the motion and consequently an appropriate vortex wake model has to be developed. Wake rollup and flowfield velocity computations are then carried out in the inertial frame of reference, whereas the moving frame of reference serves for defining the momentary boundary conditions.

The Unsteady Wake

The modeling of the vortex wake, shed from the wing's trailing edges or from user-defined separation lines, is obtained by adding wake panel elements at each time interval Δt along these lines. This representation of the wake requires a starting-type solution where at $t=0$ the body is at rest. Beginning with the first time step, the wake panels are being shed from the trailing edges or from the prescribed leading edges, as shown in Fig. 2. During the forthcoming time intervals, this wake-shedding routine continues together with a wake rollup calculation. This rollup, during the first four steps, is shown in Fig. 2 by the streamwise panel lines only (for simplicity). To achieve the vortex rollup, the wake panel corner points $(X, Y, Z)_i$ are being transported by the local velocity $(U, V, W)_i$, induced by the body and its wakes. The corresponding displacement for each time interval is

$$\begin{pmatrix} \Delta X \\ \Delta Y \\ \Delta Z \end{pmatrix}_i = \begin{pmatrix} U \\ V \\ W \end{pmatrix}_i \cdot \Delta t \tag{12}$$

This routine was used to simulate the periodic wake shedding behind separated, two-[12] and three-dimensional[13] wings and for modeling LE separation and vortex rollup over slender delta wings.[14,15] The strength of the wake panels are determined by the Kutta condition (6) and by the Kelvin condition (7). This is done such that the doublet strength of the latest wake element is equal to the local potential jump $\Phi_{\text{upper}} - \Phi_{\text{lower}}$ of the shedding panels along the trailing edges and the separation lines. This scheme, together with moving the wake elements parallel to the local streamlines (12), is the time-dependent equivalent of the Kutta condition. Since the doublet strength of each wake panel is constant, this representation is equivalent to modeling the wake by a lattice of closed vortex rings (which automatically fulfill the Kelvin condition). The physical meaning is that for any growth in the circulation of the wing, a vortex equal in magnitude and opposite in sign (created by the potential jump between the lastest and the preceeding wake elements) will be shed into the wake.

Solution of the problem

The general solution of Eq. (10) is a sum of source σ and doublet μ distribution over the body's surface and its wakes:

$$\Phi(x,y,z) = \frac{-1}{4\pi}\int_{\text{body+wake}} \left[\mu n \cdot \nabla\left(\frac{1}{r}\right) - \sigma\left(\frac{1}{r}\right)\right] \mathrm{d}s \tag{13}$$

This formulation describes both the outer flow and the body's internal flow and fulfills the boundary condition (5). However, Eq. (13) still does not uniquely describe a single solution since a large number of source and doublet distribution will satisfy a set of outer boundary conditions [Eq. (11b)]. The choice that was made here is similar to the basic approach taken in the VSAERO code.[9] That is that the instantaneous internal flow is set to be equal to the onset flow caused by the motion of the body's frame of reference. Consequently, the strength of the source at each panel on the thick body is set equal to the local onset velocity (14). This choice results in smaller values of the unknown doublets and thereby will stabilize the numerical solution

$$\sigma = -n \cdot (V_o + \Omega \times r) \tag{14}$$

Since the wake is assumed to consist of thin vorticity sheets only, no internal flow needs to be specified there, and the wake will be modeled by doublet elements only. To uniquely solve the outer flow about the body, the doublet distribution has to be determined by boundary condition [Eq. (11b)]. Therefore, Eq. (13) is derived one more time with respect to the body coordinates. The resulting velocity induced by the

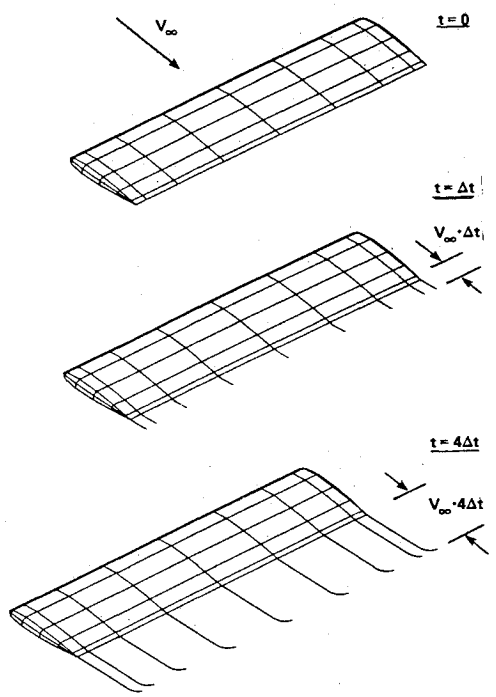

Fig. 2 The time-dependent wake-shedding procedure.

combination of the doublet and source distribution is

$$\nabla\Phi = \frac{-1}{4\pi}\int_{\text{body+wake}} \mu\nabla\left[n\cdot\nabla\left(\frac{1}{r}\right)\right]\mathrm{d}s + \frac{1}{4\pi}\int_{\text{body}} \sigma\nabla\left(\frac{1}{r}\right)\mathrm{d}s \tag{15}$$

In order to establish the boundary value problem, the local velocity at each point on the body has to satisfy the zero flow condition across the body's surface, Eq. (11a), or in the case of transpiration, Eq. (11b). By substituting this equation into the left-hand side of Eq. (15) the final integral equation is formed with the unknown μ. Since this equation is geometrically complex and also singular, the body and the wakes are divided into discrete panel elements with constant strength of σ_i or μ_i. Then for each body panel the instantaneous source value is computed by Eq. (14) while the doublet remains as the unknown. By applying the Kutta condition and constructing the wake progressively at each time interval, the strength μ_{wi} is known from previous time steps. For the first time step, therefore, no wake elements are present. As a result of this discretization, Eq. (11b) with $\nabla\Phi$ taken from Eq. (15) is derived at the centroid of each panel, resulting in the following algebraic equation:

$$[A_{ij}]\begin{pmatrix}\mu_1\\ \mu_2\\ \cdot\\ \cdot\\ \mu_k\end{pmatrix} = [B_{ij}]\begin{pmatrix}\sigma_1\\ \sigma_2\\ \cdot\\ \cdot\\ \sigma_k\end{pmatrix} + [C_{ij}]\begin{pmatrix}\mu_{w1}\\ \mu_{w2}\\ \cdot\\ \cdot\\ \mu_{wl}\end{pmatrix} + \begin{pmatrix}(v_f\cdot n)_1\\ (v_f\cdot n)_2\\ \cdot\\ \cdot\\ (v_f\cdot n)_k\end{pmatrix} + \begin{pmatrix}v_{N1}\\ v_{N2}\\ \cdot\\ \cdot\\ v_{Nk}\end{pmatrix} \tag{16}$$

The subscript $(\,)_k$ refers to the numbers of body panels whereas $(\,)_l$ is the number of wake elements that increases with each additional time step. The inlet/exit transpiration velocity v_{Ni} is determined by the programmer for the specific panels. The time-dependent motion of the (x, y, z) frame is

defined by Eqs. (1) and (2); therefore the local geometrical velocities $(v_f \cdot n)_i$ are computed with Eq. (9) and will have the form

$$-v_{f,i} = (\dot{X}_o, \dot{Y}_o, \dot{Z}_o) + (\dot{\phi}, \dot{\theta}, \dot{\psi}) \times (x, y, z) \quad (17)$$

The influence coefficients $[A_{ij}]$, $[B_{ij}]$, $[C_{ij}]$ consist of complex geometrical relations and their derivation is documented in references such as Refs. 5 or 10. The first two are a function of the body geometry only and are computed only once. The influence matrix of the wake $[C_{ij}]$ is growing with each time step and therefore requires continuous reevaluation. Once the matrix equation (16) is solved (for each time step), the resulting pressures can be computed by Bernoulli equation. In the inertial frame of reference this equation is

$$\frac{p_\infty - p}{\rho} = \frac{1}{2}\left[\left(\frac{\partial \Phi}{\partial X}\right)^2 + \left(\frac{\partial \Phi}{\partial Y}\right)^2 + \left(\frac{\partial \Phi}{\partial Z}\right)^2\right] + \frac{\partial \Phi}{\partial t} \quad (18)$$

whereas in the body-fixed frame this equation will have the form:[16]

$$\frac{p_\infty - p}{\rho} = \frac{1}{2}\left[\left(\frac{\partial \Phi}{\partial x}\right)^2 + \left(\frac{\partial \Phi}{\partial y}\right)^2 + \left(\frac{\partial \Phi}{\partial z}\right)^2\right] + (V_0 + \Omega \times r) \cdot \nabla \Phi + \frac{\partial \Phi}{\partial t} \quad (19)$$

As the pressure and the potential field are obtained, computations such as forces, moments, surface velocity surveys, etc., can be carried out.

Conversion of Panel Codes to the Unsteady Mode

Computer codes based on potential panel methods have been developed in the past two decades, and their computational efficiency has improved[17] so that complex aircraft shapes can be analyzed. Based on the above analysis, a three-step method can be devised so that a steady-state panel code will be upgraded to include the unsteady mode. These steps are as follows:

1) A time-stepping wake model, similar to the one described here, has to be utilized. This wake has to fulfill the Kelvin condition (7) and should be allowed to roll up because of the induced velocity (12).

2) The normal velocity component $(v_f \cdot n)_i$ in Eq. (16) has to include the components due to the rotations as presented by Eq. (17).

3) The above correction of the local velocities must be included in the pressure calculations and a modified Bernoulli's equation (19) should be used.

These principles were previously applied to helicopter rotor-tip shape study[4] and to a slender wing model[18] where two-dimensional, longitudinal motions were analyzed. In this current study, similar principles are applied to a panel-computer-code (VSAERO[9]), and three-dimensional motions and aircraft configurations are investigated.

Test Cases and Examples

As a first example, the sudden acceleration of a wing that initially was at rest (as in Fig. 2) is investigated. The motion of the (x, y, z) frame at $t > 0$ is then given by Eq. (1):

$$G_1 = V_\infty \begin{pmatrix} 1 \\ 0 \\ 0 \end{pmatrix} t, \quad (\text{for } t > 0) \quad (20)$$

The kinematic velocity v_f in Eq. (17) is then reduced to

$$v_{f,i} = -V_\infty \begin{pmatrix} 1 \\ 0 \\ 0 \end{pmatrix}, \quad (\text{for } t > 0) \quad (21)$$

so that by substituting Eq. (21) into Eq. (16), the solution at each time step is obtained. Computed results for both the classical two-dimensional case[19] and for a finite, rectangular wing ($AR = 6$) compares well with previous computations[19,20] (see Fig. 3). Similar computation for a complex aircraft shape is presented in Fig. 4, whereas the geometrical details of the aircraft are presented in Fig. 5. The canard was horizontal, but the wing had an anhedral of 2 deg 46′. More information on the geometry of this model is provided in Refs. 21–23. The panel model of this configuration consists of 706 panels per one side of the model. During the wind-tunnel tests[21–23] with this model, a free airflow across the inlet was monitored. To simulate this condition a normal inflow velocity of $v_N = -V_\infty$ was specified at the inlet. To conserve the internal mass flow rate, an exit velocity of $v_N = 0.55V_\infty$ was specified, in a similar manner, at the exhaust plane in the base of the fuselage.

The transient lift growth of the wing/canard combination, presented in Fig. 4, differs somewhat from the monotonic lift increase of a single lifting surface[24] (Fig. 3). At the first moment the lift of the wing and canard grow at about the same rate, with the lift of the wing being slightly lower because of the canard-induced downwash. Then the wing's lift increases beyond its steady state value, since the canard wake has not yet reached the wing. At about $V_\infty t/c \approx 1.0$ the canard wake reaches the wing and its influence begins to reduce the wing's lift. This behavior results in the lift-overshoot, as shown in Fig. 4.

The flexibility of this method can be demonstrated by rotating a pair of high-aspect-ratio, untwisted wings along the

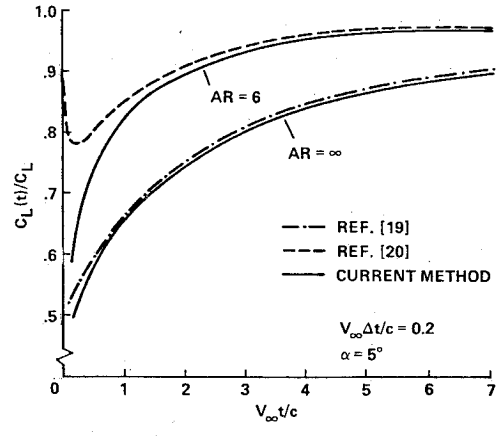

Fig. 3 Lift coefficient variation after a plunging motion of a rectangular wing.

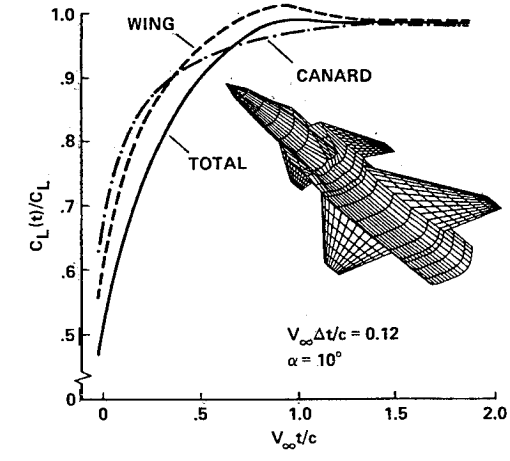

Fig. 4 Lift coefficient variation after a plunging motion of a complete aircraft configuration.

z axis, to simulate rotor aerodynamics. The trailing-edge vortices behind this two-bladed rotor, which was impulsively set into motion, are presented in Fig. 6. Similar information on wake trajectory and rollup, for more complex rotorcraft geometries and motions (including forward flight), can easily be calculated by this technique. This information can then be utilized for vehicle stability and aerodynamic studies, and as a far-field information for more complex, regional viscous computer codes.[25] Computation methods, with similar capabilities to those shown by Fig. 6, have been developed before.[26-30] However, all these computations were limited to geometries of rotor-like shapes, whereas the current method is capable of treating both fixed-wing and rotor configurations.

The spanwise lift distribution on one rotor blade of Fig. 6, after one-quarter revolution ($\Delta\psi = 90$ deg), is presented in Fig. 7. The rotor for this example was untwisted and had a collective pitch angle of $\alpha_R = 8$ deg, to duplicate the geometry of the rotor tested by Caradona and Tung.[31] The large difference between this spanwise loading ($\Delta\psi = 90$ deg) and the experimental loading measured in Ref. 31, for a hovering rotor, are due to the undeveloped wake. This solution can be considerably improved by adding a far-wake model.[30] To model the far wake correctly, for the hover case, several rotations are needed to construct the spiral vortex tube beneath the rotor. Since the array sizes of this pilot code were kept small, for faster turnaround times, only 30 time steps were possible without further modifications to the computer program. Consequently, only the coarse, near-wake shape shown in Fig. 8 was constructed by simply rotating the model with larger time steps, allowing about three complete revolutions. Because of these large time steps, wake deformation (and contraction) was minimal. Also, for the initial downward motion of the wake, a far-wake-induced velocity of about $R\dot{\psi}\alpha$ (for the wake only) was assumed. The downwash induced by the spiral vortex wake of Fig. 8 reduced the spanwise lift distribution on the wake to values that are close to those measured by Caradona and Tung,[31] as shown in Fig. 7 (by the "steady hover" line). The corresponding chordwise pressures, for three blade stations, are presented in Fig. 9. The computed pressures fall close to the measurements of Ref. 31, and the small deviations could be a result of the sparse panel grid used or could be due to experimental errors.

Basic unsteady aerodynamic test cases, in addition to the plunging motion, usually include heave and pitch oscillations.[20,32] Computed results for the lift variations during a heaving oscillation cycle with an amplitude of $h/c = 0.1$, for an $\mathcal{R} = 4$ rectangular wing with a NACA 0012 airfoil section, is presented in Fig. 10. The results of the computation

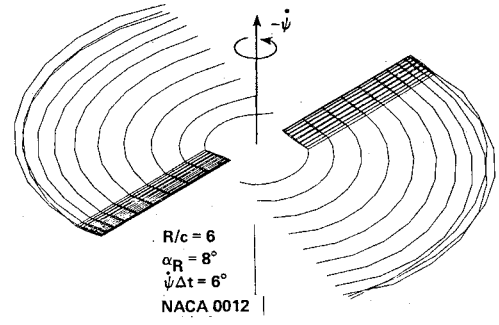

Fig. 6 Two-bladed rotor and its wake, after one-quarter revolution.

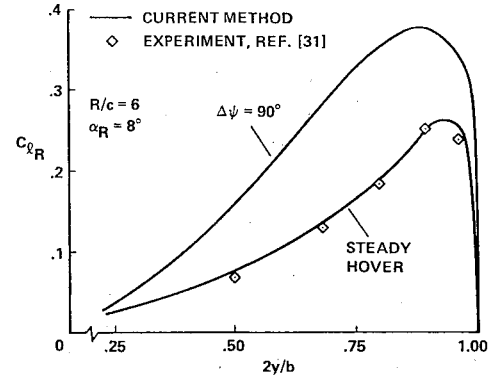

Fig. 7 Spanwise lift distribution on a helicopter blade.

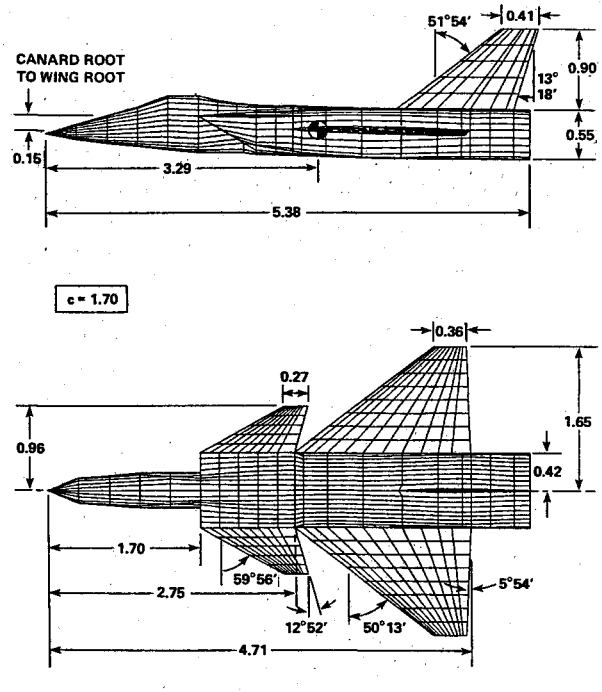

Fig. 5 Geometric details of the aircraft model (dimensions in meters).

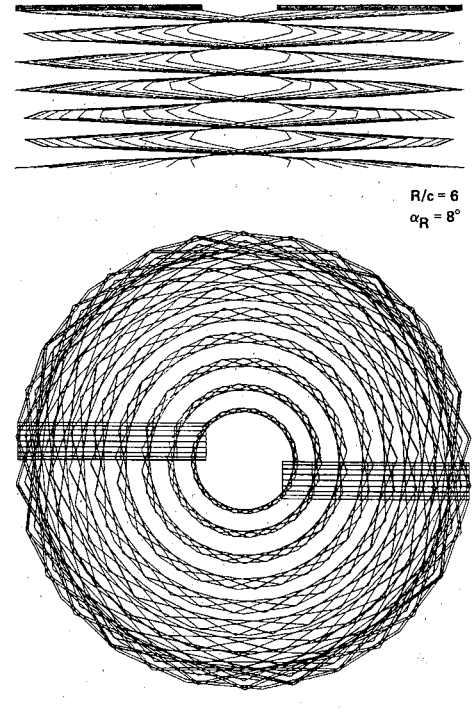

Fig. 8 Front and top views of a hovering helicopter rotor and its wake.

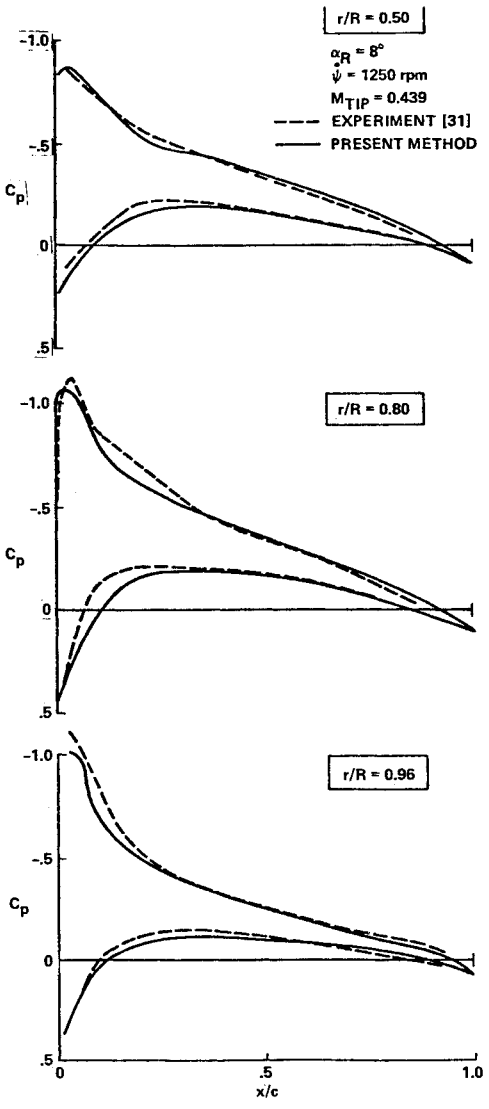

Fig. 9 Chordwise loading at different sections of a hovering rotor.

agree well with the vortex-lifting-surface computations of Ref. 20. The advantage of the current panel method is that the same computations can be carried out on more complex aircraft shapes, as shown in Fig. 11. Here the aircraft model undergoes similar heaving oscillation and the resulting time-dependent lift is presented. The small delay in the lift, relative to the motion's phase angle is a result of the delayed influence of the canard wake on the wing, whose lift lags slightly behind. The computed wake lines behind the moving aircraft are shown in the inset to Fig. 11 and even with the coarse time steps (28 per cycle), reasonable wake rollup is observed.

Lift and pitching moment histograms, during a large-amplitude pitch oscillation cycle, of a two-dimensional airfoil are presented in Fig. 12. Comparison is made with experimental results of Ref. 33 for oscillations about the airfoil's quarter chord. The computations are reasonably close to the experimental values of the lift coefficient through the cycle. During the pitchdown motion, however, a limited flow separation reduces the lift of the airfoil in the experimental data. Similar computations, with a two-dimensional panel method, were reported in Ref. 34. The shape of the pitching-moment histogram is close to the experimental result with a small clockwise rotation. This is a result of the inaccuracy of computing the airfoil's center of pressure, since only nine chordwise panels were used.

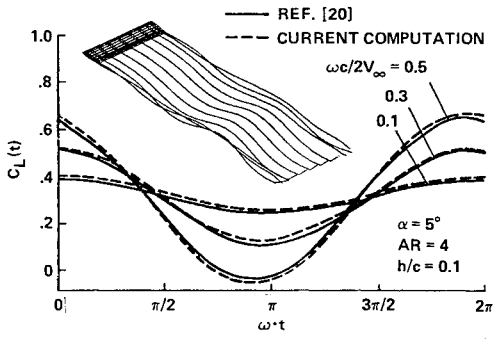

Fig. 10 Periodic lift variation during heaving oscillations of an $\mathcal{R} = 4$ rectangular wing (with NACA 0012 section).

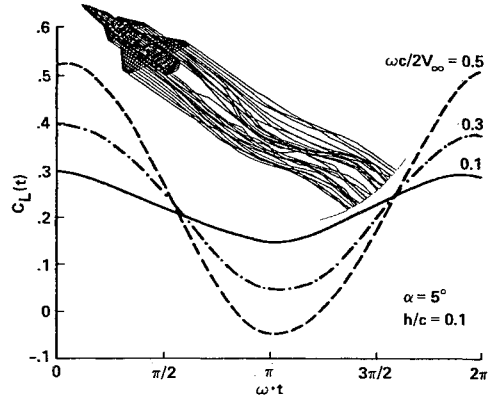

Fig. 11 Periodic lift variation during heaving oscillations of a complete aircraft configuration.

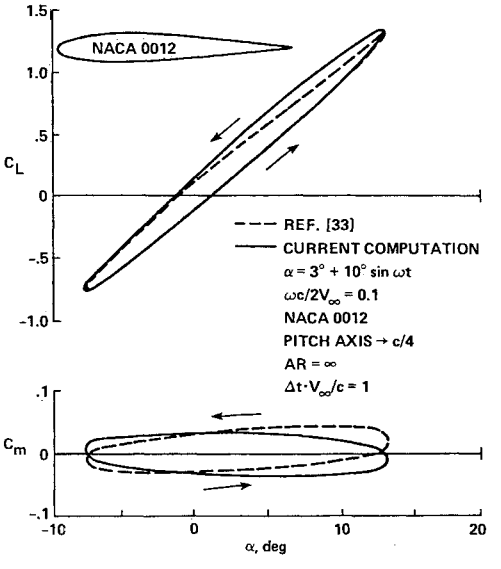

Fig. 12 Lift and pitching-moment histogram for the pitch oscillations of a NACA 0012 airfoil.

Similar histograms for the complex aircraft shape of Fig. 5 are presented in Fig. 13. The pitching motion is about the assumed center of gravity, as shown in Fig. 5. The direction of rotation in the pitching-moment diagram is reversed because of the interaction between the canard wake and the wing. One of the mentioned advantages of this method is the capability of computing aircraft stability derivatives. This can be demonstrated by applying the formulation for the damping

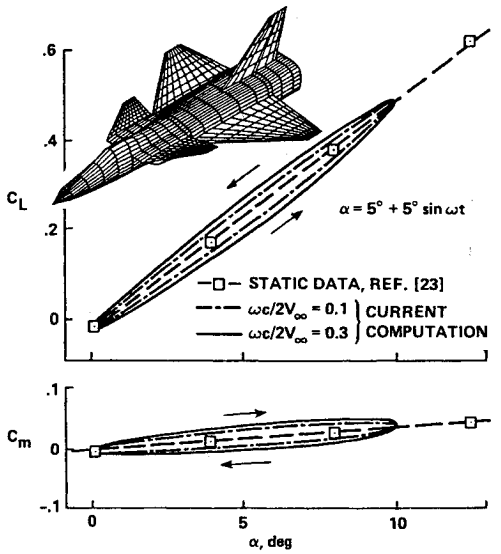

Fig. 13 Lift and pitching-moment histogram for the pitch oscillations of the complete aircraft configuration.

coefficient[35] to the data presented in Figs. 12 and 13:

$$C_{m\dot{\alpha}} = \frac{\partial C_m}{\partial\left(\frac{\dot{\alpha}c}{2V_\infty}\right)} = \frac{2V_\infty}{\omega c}\frac{1}{\pi\alpha_1}\int_0^{2\pi} C_m(t)\cos(\omega t)\,\mathrm{d}(\omega t) \tag{22}$$

Here the integration is performed over the whole pitch oscillation cycle, with α_1 being the amplitude of the pitch oscillations. The pitch-damping coefficients, obtained by Eq. (22) for the NACA 0012 airfoil (by analyzing the pitching moment histogram in Fig. 12) and for the complete aircraft configuration (from Fig. 13), are estimated to be 0.032/deg and −0.012/deg, respectively.

Simulation of flow separation from wings with highly swept LE, by the time-stepping method, is demonstrated in Fig. 14. This is obtained by gradually releasing vortex wake panels from the sharp LE, similarly to the wake-shedding process at the trailing edge, until the fully developed wake shape is obtained. The vortex rollup is determined by the momentary velocity, induced by the wing and its wakes (Eq. 12). Results for the lift curve of this delta wing are presented in Fig. 15. At the lower angles of attack (less than ~10 deg), the lift curve slope is well predicted by the linear formulation of Jones[36] [$C_L = (\pi \mathcal{R}/2)\alpha$]. At higher incidences, however, the LE vortices increase the lift, as indicated by a sample of experimental results.[37-39] This vortex lift is not predicted by the basic linear panel method[9] since the LE wake is not included. The addition of the separated LE vortex model in this current method (shown in Fig. 15) increases the wing's lift and improves the comparison with the experimental data. At very high angles of attack (above 40 deg), however, vortex breakdown results in the wing's lift loss, a condition that is not modeled here.

The spanwise pressure distribution at the $x/c = 0.5$ station is presented in Fig. 16. The wing model consists of 248 panels with 12 spanwise equally spaced panels, and the nondimensional time step was 0.1 chord ($V_\infty \Delta t/c = 0.1$). Results for a denser computation grid (328 panels, 16 spanwise panels, $V_\infty \Delta t/c = 0.05$) are presented by the solid line, and both computations show the suction peaks resulted by the LE vortices. The experimental results with the turbulent boundary layer of Ref. 40 ($Re = 0.9 \times 10^6$ for both experiments) indicate a secondary vortex near the LE which was not modeled here. In general, it was found that the lift of the delta wing was less sensitive to coarse grid and time steps than the pressure distribution over the wing's surface. In cases when computer time saving is considered and larger time steps are

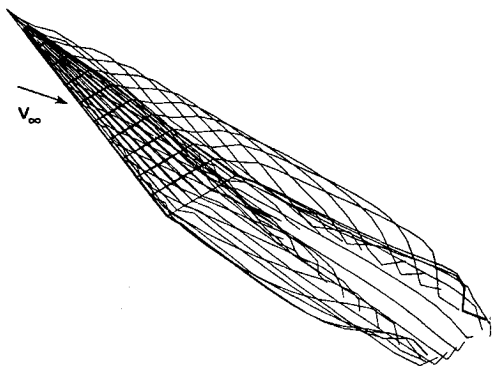

Fig. 14 Simulation of LE separation by releasing vortex sheets from the separation lines.

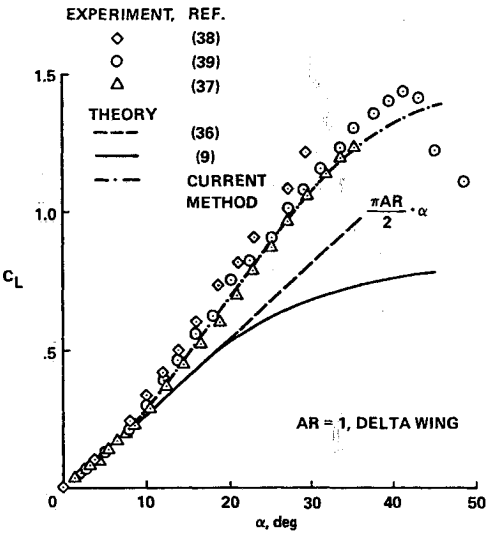

Fig. 15 Experimental and computed lift curves for an $\mathcal{R} = 1$ delta wing.

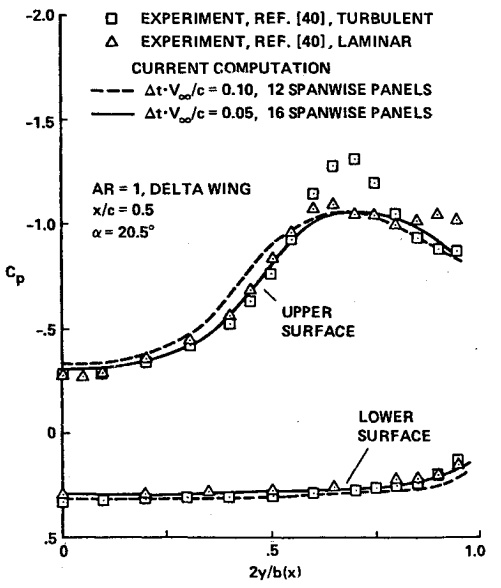

Fig. 16 Spanwise loading of a delta wing (at $x/c = 0.5$).

applied, the spanwise pressure distribution would smear, but the lift will change by only a few percent.

For demonstrating more complex motions, the wake lines behind a delta wing having an aspect ratio of 0.71, undergoing a coning motion, is presented in the inset of Fig. 17. The wing

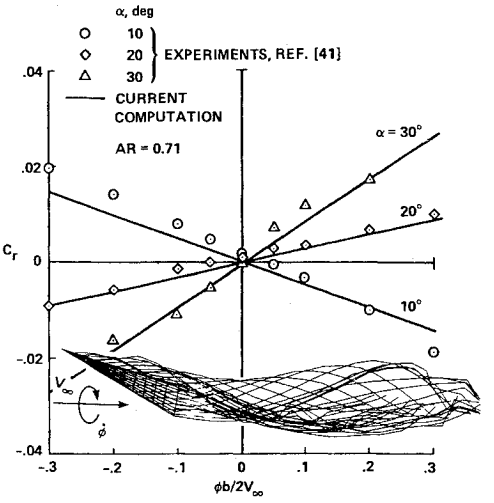

Fig. 17 Rolling moment vs coning rate for a delta wing in a coning motion.

angle of attack α was set relatively to the x, y, z frame of reference (pitching along $x/c = 0.6$) and then was rotated about the x axis at the rate ϕ. Computed rolling moments are compared with experimental data of Ref. 41 in Fig. 17. The slopes of the computed rolling moment curves, which change rapidly with variations of angle of attack, compare reasonably well with the experiments. For angles of attacks higher than 30 deg and for roll rates $\phi b/2V_\infty$ larger than 0.1, vortex breakdown bends the experimental curves and larger differences between the experiment and the computation are detected.

Conclusions

The basic unsteady formulation of potential flow was derived and applied to a first-order panel method (with constant singularity for each element). Some of the capabilities of this approach were demonstrated by this pilot code on a variety of simple examples. The method in its current state can be utilized for computing longitudinal, lateral, and cross-coupled stability derivatives for actual aircraft shapes, where prediction by experiments and other methods is still very limited. Vortex wake dynamics can be studied, as well, for a variety of difficult problems, such as aircraft spin entry, spin alleviation, or helicopter blade/body interaction.

Because of the limited number of wake elements at this stage of the code development, large time steps were used. Therefore, in the case of the rotor wake rollup and oscillatory motions, some of the finer interactions were smoothed out. Even so, the computed results agree well with the experimental data that were presented for some of the test cases. Consequently, immediate refinements of this computer program will concentrate on increasing the wake array size. Additionally, cases with relative component motion will be considered. These cases will include rotor rotation, relative to the helicopter fuselage, or time-dependent variation of aircraft wing geometry.

Future development of this method needs to include interaction with viscious methods based on a regional approach. This will allow the investigation of fluid dynamic conditions involving lifting jets of V/STOL aircraft, boundary layers, and flow separations.

References

[1]Chapman, D.R., "Computational Aerodynamics Development and Outlook," *AIAA Journal*, Vol. 17, Dec. 1979, pp. 1293–1313.

[2]Woodward, F.A., "Analysis and Design of Wing-Body Combinations at Subsonic and Supersonic Speeds," *Journal of Aircraft*, Vol. 5, June 1968, pp. 528–534.

[3]Hess, J.L. and Smith, A.M.O., "Calculation of Potential Flow About Arbitrary Bodies," *Progress in Aeronautical Sciences*, Vol. 8, Pergamon Press, 1967, pp. 1–138.

[4]Maskew, B., "Influence of Rotor Blade Tip Shape on Tip Vortex Shedding—An Unsteady Inviscid Analysis," *Proceedings of the 36th Annual Forum of the American Helicopter Society*, May 1980.

[5]Hess, J.L., "Calculation of Potential Flow About Arbitrary Three-Dimensional Lifting Bodies," J5679-01, Final TR MDC, McDonnell Douglas, Long Beach, CA, Oct. 1972.

[6]Woodward, F.A., "An Improved Method for the Aerodynamic Analysis of Wing-Body-Tail Configurations in Subsonic and Supersonic Flow," NASA CR-2228, May 1973.

[7]Morino, L., "A General Theory of Unsteady Compressible Potential Aerodynamics," NASA CR-2464, 1974.

[8]Carmichael, R.L. and Ericson, L.L., "PAN AIR—A Higher Order Panel Method for Predicting Subsonic or Supersonic Linear Potential Flows About Arbitrary Configurations," AIAA Paper 81-1255, June 1981.

[9]Maskew, B., "Program VSAERO, A Computer Program for Calculating the Nonlinear Aerodynamic Characteristics of Arbitrary Configurations," NASA CR-166476, Nov. 1982.

[10]Johnson, F.T., "A General Panel Method for the Analysis and Design of Arbitrary Configurations in Incompressible Flows," NASA CR-3079, May 1980.

[11]Maskew, B., Strash, D., Nathman, J., and Dvorak, F.A., "Investigation to Advance Prediction Techniques of the Low-Speed Aerodynamics of V/STOL Aircraft," NASA CR-166479, Feb. 1983.

[12]Katz, J., "A Discrete Vortex Method for the Non-Steady Separated Flow Over an Airfoil," *Journal of Fluid Mechanics*, Vol. 102, 1981, pp. 315–328.

[13]Katz, J., "Large Scale Vortex-Lattice Model for the Locally Separated Flow Over Wings," *AIAA Journal*, Vol. 20, Dec. 1982, pp. 1640–1646.

[14]Levin, D.C. and Katz, J., "Vortex Lattice Method for the Calculation of the Nonsteady Separated Flow over Delta Wings," *Journal of Aircraft*, Vol. 18, Dec. 1981, Dec. 1981, pp. 1032–1037.

[15]Katz, J., "Lateral Aerodynamics of Delta Wings with Leading Edge Separation," *AIAA Journal*, Vol. 22, March 1984, pp. 323–328.

[16]Katz, J. and Weihs, D., "Hydrodynamics Propulsion by Large Amplitude Oscillation of an Airfoil with Chordwise Flexibility," *Journal of Fluid Mechanics*, Vol. 88, pt. 3, 1978, pp. 485–497.

[17]Margason, R.J., Kjelgaard, S.O., Sellers, W.L., III., Morris, C.E.K., Jr., Walkey, K.B., and Shields, E.W., "Subsonic Panel Methods–A Comparison of Several Production Codes," AIAA Paper 85-0280, Jan. 1985.

[18]Katz, J., "Method for Calculating Wing Loading During Maneuvering Flight along a Three-Dimensional Curved Path," *Journal of Aircraft*, Vol. 16, Nov. 1979, pp. 739–741.

[19]Wagner, H., "Uber die Entstehung des Dynamischen Autriebes von Tragflugeln," *Z.F.A.M.M.*, Vol. 5, No. 1, Feb. 1925, pp. 17–35.

[20]Katz, J., "Calculation of the Aerodynamic Forces on Automotive Lifting Surfaces," *ASME Journal of Fluids Engineering*, Vol. 107, 1985, pp. 438–443.

[21]Stoll, F. and Minter, E.A., "Large-Scale Wind Tunnel Tests of a Sting-Supported V/STOL Fighter Model at High Angles of Attack," AIAA Paper 81-2621, Dec. 1981.

[22]Stoll F. and Koenig, D.G., "Large-Scale Wind-Tunnel Investigation of a Close-Coupled Canard-Delta-Wing Fighter Model Through High Angles of Attack," AIAA Paper 83-2554, Oct. 1983.

[23]Stoll, F. and Koenig, D.G., "Low-Speed Wind-Tunnel Measurements of a Canard Controlled Fighter Model Through High Angles of Attack," NASA TMX 84403, 1986.

[24]Levin, D., "A Vortex-Lattice Method for Calculating Lifting-Surface Interference," AIAA Paper 81-1662, Aug. 1981.

[25]Davis, S.S. and Chang, C., "The Critical Role of Computational Fluid Dynamics in Rotary-Wing Aerodynamics," AIAA Paper 86-0336, Jan. 1986.

[26]Johnson, W., *Helicopter Theory*, Princeton University Press, Princeton, NJ, 1980.

[27]Crispin, Y., "Unsteady Rotor Aerodynamics Using a Vortex Panel Method," AIAA Paper 82-1348, Aug. 1982.

[28]Miller, R.H., "Application of Fast Free Wake Analysis Techniques to Rotors," *Vertica*, Vol. 8, No. 3, 1984, pp. 255–261.

[29]Morino, L., Kaprielian, Z., Jr., and Sipcic, S.R., "Free Wake Analysis of Helicopter Rotors," *Vertica*, Vol. 9, No. 2, 1985, pp. 127–140.

[30]Summa, J.M., "Advanced Rotor Analysis Methods for the Aerodynamics of Vortex-Blade Interactions in Hover," *Vertica*, Vol. 9, No. 4, 1985, pp. 331–343.

[31]Caradonna, F.X. and Tung, C., "Experimental and Analytical Studies of a Model Helicopter Rotor in Hover," NASA TM-81232, 1981.

[32]Katz, J., and Weihs, D., "Wake Rollup and the Kutta Condition for Airfoils Oscillating at High Frequency," *AIAA Journal* Vol. 19, Dec. 1981, pp. 1604–1606.

[33]McCroskey, W.J., McAlister, K.W., Carr, L.W., Pucci, S.L., Lambert, O., and Indergrand, R.F., "Dynamic Stall on Advanced Airfoil Sections," *Journal of the American Helicopter Society*, July 1981, pp. 40–50.

[34]Maskew, B. and Dvorak, F.A., "Prediction of Dynamic Stall Characteristics Using Advanced Nonlinear Panel Methods," *Proceedings of AFOSR/FJSRL Workshop on Unsteady Separated Flow*, Aug. 1983.

[35]Katz, J. and Schiff, L.B., "Modeling Aerodynamic Response to Aircraft Maneuvers—A Numerical Validation," *Journal of Aircraft*, Vol. 23, Jan. 1986, pp. 19–25.

[36]Jones, R.T., "Properties of Low Aspect-Ratio Pointed Wings at Speeds Below and Above the Speed of Sound," NACA Rept. 835, 1946.

[37]Peckham, D.H., "Low-Speed Wind-Tunnel Tests on a Series of Uncambered Slender Pointed Wings with Sharp Edges," R.A.E. Aero. Rept. 2613, 1958.

[38]Davenport, E.E. and Huffman, J.K., "Experimental and Analytical Investigation of Subsonic Longitudinal and Lateral Aerodynamic Characteristics of Slender Sharp-Edge 74 deg Swept Wings," NASA TN D-6344, 1971.

[39]Levin, D. and Katz, J., "Dynamic Load Measurements with Delta Wings Undergoing Self-Induced Roll Oscillations," *Journal of Aircraft*, Vol. 21, 1984, pp. 30–36.

[40]Hummel, D., "On the Vortex Formation Over a Slender Wing at Large Angles of Incidence," Paper No. 15, *High Angle of Attack Aerodynamics*, AGARD CP-247, Oct. 1978.

[41]Nguyen, L.T., Yip, L., and Chambers, J.R., "Self-Induced Wing Rock of Slender Delta Wings," AIAA Paper 81-1883, Aug. 1981.